Int. J. Electrochem. Sci., 11 **(2016)** 6735 – 6746, doi: 10.20964/2016.08.12

International Journal of ELECTROCHEMICAL SCIENCE
www.electrochemsci.org

Synergistic Electronic Pull of Graphene Oxide Supported Pd Nanoparticles on Enhancing Catalytic Activity of Electro Deposited Pt Nanoparticles for Methanol Oxidation Reaction

Ammar Bin Yousaf [1,§,*], *Rashid Khan* [2,§], *Muhammad Imran* [1], *Carlos Fernandez* [3], *Cheng-Zong Yuan* [1] *and Li Song* [2]
[1] Hefei National Laboratory for Physical Sciences at Microscale, School of Chemistry and Material Sciences, University of Science and Technology of China, Hefei 230026, P. R. China
[2] National Synchrotron Radiation Laboratory, CAS Canter for Excellence in Nanoscience, University of Science and Technology of China, Hefei 230029, P. R. China
[3] School of Pharmacy and Life Sciences, Sir Ian Wood Building, Robert Gordon University, AB10 7GJ Aberdeen, UK
[§]These two authors contributed equally to this work
[*]E-mail: ammar@mail.ustc.edu.cn

Received: 25 April 2016 / *Accepted:* 29 May 2016 / *Published:* 7 July 2016

Graphene oxide supported clean Pd nanoparticles were synthesized by using CO as a reducing agent. Pt film was deposited on Pd NPs through electrochemical potential cycling method. The as-developed catalyst, which exhibits higher catalytic performance for electro oxidation of methanol and better tolerance to the CO poisoning effect suffered during methanol oxidation reaction (MOR). The higher performance of catalyst attribute towards the long chain organic capping agent free formation process of clean PdPt nanocomposite. This facile and effective route is of great significance for the synthesis of Pd-based catalysts on electrode surface directly with highest MOR activity. The synergistic electronic pull provided by graphene oxide supported Pd nanoparticles to Pt in the composite material highly enhanced the electro catalytic activity.

Keywords: Pd Nanoparticles, Pd-Pt Nanocomposite, graphene oxide support, electrochemical deposition, synergistic effect, methanol oxidation reaction

1. INTRODUCTION

Direct alcohol fuel cells are strong candidates and expected to play a major contributions in the development of sustainable technologies that lower the depletion of fossil fuels, which in terms of mitigate global warming issues [1,2]. Direct methanol fuel cells (DMFCs) are attractive power source devices, the higher energy density of methanol and lower operating temperature of DMFCs are their

most common advantages [3]. Among the noble metals, the Pt and Pt-based alloys electro-catalysts are the widely used anodes in DMFCs. The commercialization of DMFCs still remained a challenging task due to the economically unfriendly cost of Pt and its saver poisoning issue by the intermediate carbonaceous species such as, CO_{ads} formed during the methanol oxidation [4]. Reformation of alternative materials with their high performance as DMFCs anodes and economically favorable low-cost electrocatalysts research is indeed of great attention.

Recently, PdPt based bimetallic electro-catalysts have been considered as auspicious choice because of the comparatively low-cost of Pd and greater resistance to CO adsorption over catalysts's active sites rather than the pure Pt anodes in DMFCs [5]. As for the nucleation of nanoparticles (NPs) on reduced graphene oxide (GO) support material, the results revealed that Pd atoms could interact with more strongly to graphene oxide to develop their intimate contact with conductive support material. The as-developed strong-metal-support-interaction (SMSI) leads to the generation of more coordination and transference of electrons between them [6]. This information provides a new direction for the synthesis of Pd-based nanocatalysts, the graphene oxide could be a most favorable substrate [7].

Electrochemical fabrication of metallic NPs is the robust technique for controlled and low-content deposition of desired metals onto the metal substrate, which can monitor the optimized size, density and shape of deposited NPs [8]. In this article, we demonstrate that Pt NPs film can be directly fabricated onto graphene oxide supported Pd NP at the surface of glassy carbon electrode (GCE) via potential cycling electro-deposition method. In comparison to the catalysts, chemically fabricated by applying long chain organic surfactants as capping agents, the electrodeposited catalyst revealed an unusually high catalytic activity for methanol electro-oxidation phenomenon in an acidic medium.

2. EXPERIMENTAL SECTION

2.1. Chemicals and Materials

H_2PdCl_4 (99.9 % metal basis, from Alfa Aesar), H_2PtCl_6(40% fromFluka), $HClO_4$ (from Sigma Aldrich), CH_3OH (99.9% from J.T. Baker) and CO gas (99.9% purity). All reagents were used as received without further purification.

2.2. Synthesis of Graphene Oxide Supported Clean Pd Nanoparticles

The catalyst support, reduced graphene oxide was synthesized through the reduction of graphite oxide by $NaBH_4$. GO was prepared by the modified Hummers and Offenmans method. The as-synthesized rGO powder was dispersed in water (1mg/1mL) and ultrasonicated for 30 minutes to obtain their colloidal suspension. Afterwards, 1 mM of H_2PdCl_4 solution was added in rGO colloidal dispersion. Reaction flask was vacuumed, sealed and heated at room temperature with continues stirring and controlled-flow of carbon monoxide as reducing and capping agent for 30 minutes. The resulting product of clean rGO-Pd NPs were obtained and used as such for catalytic application. There

was no need to wash the nanoparticles because no any organic ligands or reducing chemicals were used during synthesis, only CO was used as both reducing and capping agent. The adsorbed CO on NPs surface was removed by potential cycling in electrochemical experiments.

2.3. Characterization

The crystallite structure, size and morphology of synthesized rGO-Pd NPs were characterized by scanning electron microscopy (SEM), powder X-ray diffraction (XRD) (the measurements were performed with an X'pert PRO instrument, PANalytical, using Cu Kα radiation λ = 0.15418 nm), UV-vis spectroscopy (within the range of 200nm to 800nm) and Cyclic Voltammetry (CV).

2.4. Electrochemical Experiments

Before all electrochemical experimental work, a glassy carbon (GC) electrode (0.196 cm^2 geometric surface area) was polished with alumina slurries (Al_2O_3, 0.05 μm), followed by ultrasonication in 0.1 M HNO_3, 0.1 M H_2SO_4, and pure water for the time of 10 min, successively. To prepare a working electrode, 15 μL of the 1 mg/mL catalyst suspension in pure water was pipetted on the pre-cleaned GC electrode surface by a microliter pipette, after drying in vacuum at room temperature, the catalyst was covered with a thin layer of Nafion (0.1 wt % in water, 5 μL) to ensure the strong binding of catalyst onto GCE surface. Voltammetric measurements were carried out with a CHI 750D electrochemical workstation. The electrode prepared above was used as the working electrode. The Ag/AgCl (in 3 M NaCl, aq.) combination isolated in a double junction chamber and a Pt coil were used as the reference and counter electrodes, respectively. All the measurements were measured in electrochemical experiments with respect of standard values of reversible hydrogen electrode (RHE). The current densities in all results were presented with respect to the geometric surface area of the GCE which was 0.196cm^2. The experimental work for electrochemical behavior of as-developed materials was done by potential cycling (CV) test between 0.05 V to 1.2 V vs RHE at 50 mV/s scan rate and chronoamperometric tests at two constant potentials 0.50 V and 0.60 V up to 300 seconds. The as-synthesized graphene oxide supported Pd catalyst was referred as Pd-rGO and after electro-deposition of Pt on Pd-rGO was referred as Pt@Pd-rGO in all presented results. Moreover, their electrocatalytic performance for MOR was compared with commercial 20% wt Pt/C catalyst.

2.5. Electrochemical deposition of Pt on rGO-Pd NPs

The electrochemical deposition of Pt was carried out at room temperature in 0.1mM H_2PtCl_6 + 0.1M $HClO_4$ solution by potential cycling within potential range of 0.05V to 0.40V vs RHE at 50 mV/s scan rate with 20 sweep segments. After deposition, the electrode was thoroughly rinsed with Mili-Q water and then tested in 0.1 M $HClO_4$ acidic electrolyte within potential range between 0.00 V to 0.70 V at 50 mV/s vs RHE. The as-developed electro-catalyst loaded at the surface of GCE is demonstrated as Pt@rGO-Pd.

3. RESULTS AND DISCUSSION

The nucleation of Pd NPs on GO was carried out with driving force provided by the difference between oxidation and reduction potentials of GO and $PdCl_4^{2-}$ respectively. After the reaction C-C bonds remain unchanged while the C-O (from oxygen containing groups on GO) bonds reduced. The electrons for the reduction of these bonds were provided by CO (reducing agent). The carboxylic functional groups on the surface of GO may reduced by the successive growth of Pd NPs on GO surface. Therefore, it is concluded that the spontaneous deposition of Pd NPs on GO is ascribed to the to the overall reduction of GO support [10], which is as-similar to the reaction mechanism between Pt NPs and single-walled carbon nanotubes proposed by D. W. Goodman et al [11].

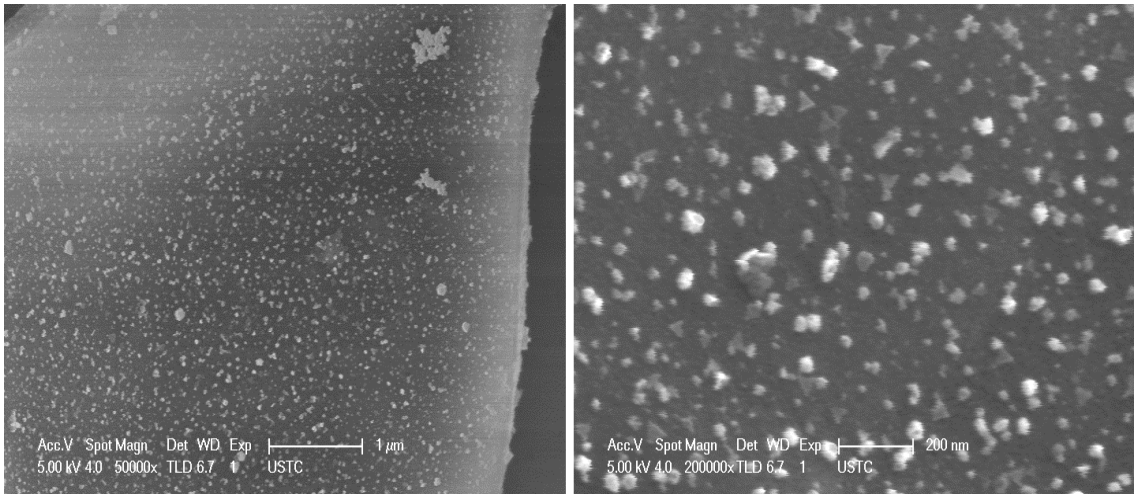

Figure 1. SEM images for Pd NPs supported on rGO, at two different magnifications.

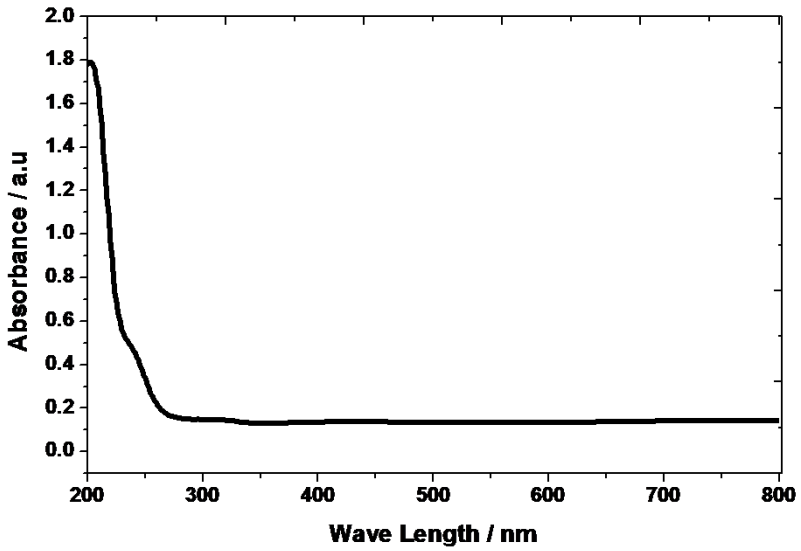

Figure 2. UV-vis spectra for Pd NPs supported on rGO.

The growth of Pd NPs during nucleation process might involve a galvanic-reaction in which the reduction of Pd atoms occurs on pre- adsorbed Pd nuclei by the electrons transferred from carboxylic species on GO surface and CO reducing agent. The above phenomenon completely described the reducing agent role of CO. As far as the capping agent role is concerned, it is documented that CO it self recognized as a poisoning specie for Pd and Pt catalysts due to its strong adsorption on the surfaces of Pd and Pt active sites. This phenomenon has been well-studied by surface scientists that, CO adsorb on various surfaces of Pd in vacuumed environment [9-13]. Due to the strong binding/ adsorption to the Pd atoms, CO may act as capping agent that facilitates the nucleation of Pd atoms restricted within desired facets of NPs. Among the comparison of CO and halides, the advantage of CO adsorbate is that it can be removed completely from the surface of metals by applying a high temperature or an electrochemical potential cycling within specified oxidation potentials, which makes it easy to un-block the active sites of as-prepared CO-adsorbed nanocrystals.

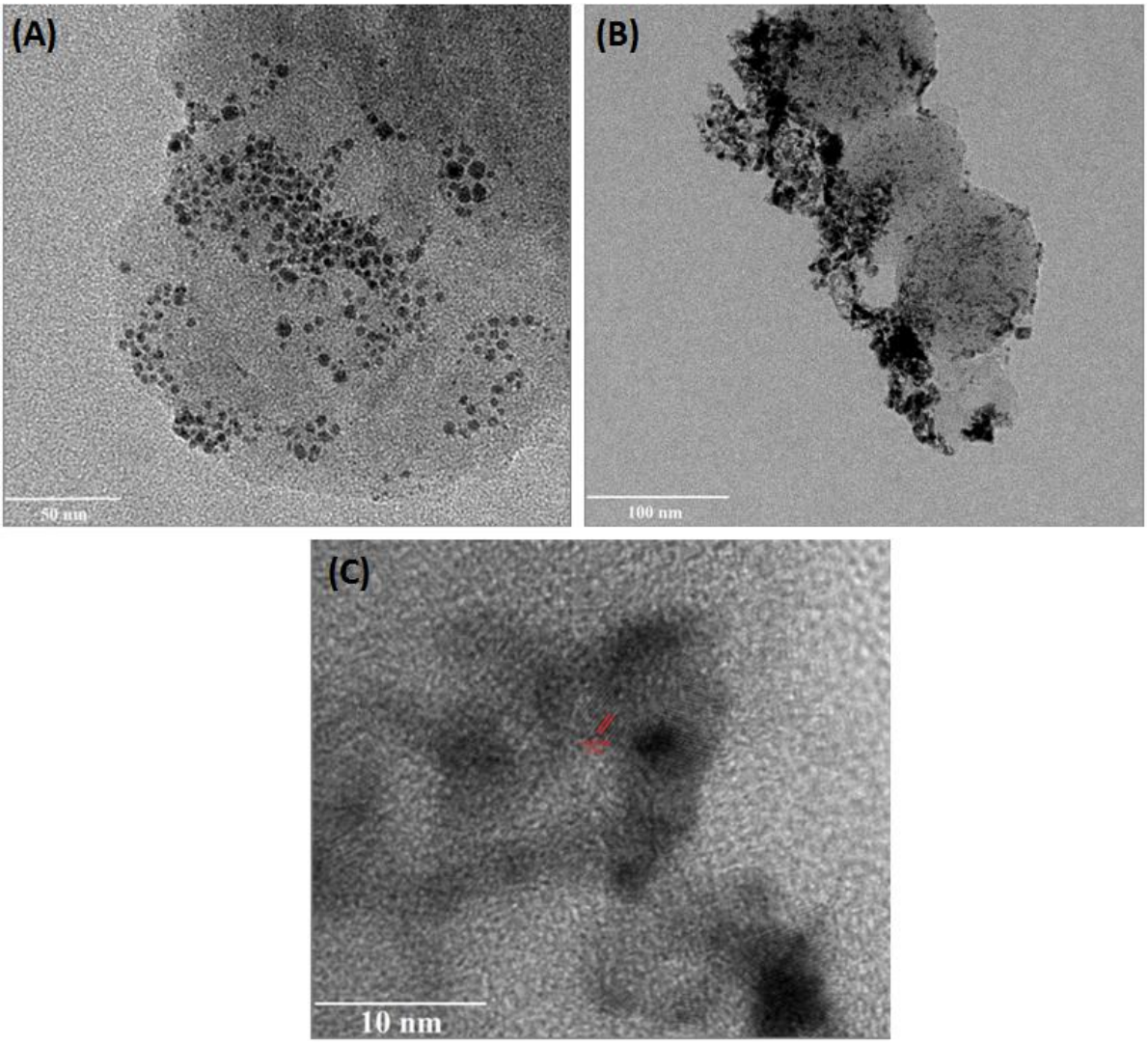

Figure 3. TEM images of (a) Pd-rGO, (b) Pt@Pd-rGO and (c) HRTEM image of Pt@Pd-rGO

SEM images presented in Figure 1, strongly verify well dispersed Pd NPs on graphene oxide. Moreover, UV-vis spectra presented the characterized absorption behavior of Pd NPs, presented in Figure 2. Despite of capping and reducing agent behavior of CO, a variety of experimental techniques have been employed, which provided the proof of CO adsorption on Pd(111) facets[14-20].N. M. Martin *et al* has also presented results that the adsorption sites occupied by CO on the different surfaces change from the hollow and bridge sites on clean Pd(111) to bridge and atop sites on the oxidized Pd surfaces [21]. All previous studies showed that the surface structure of CO overlayers on Pd(111) facets is carried out.

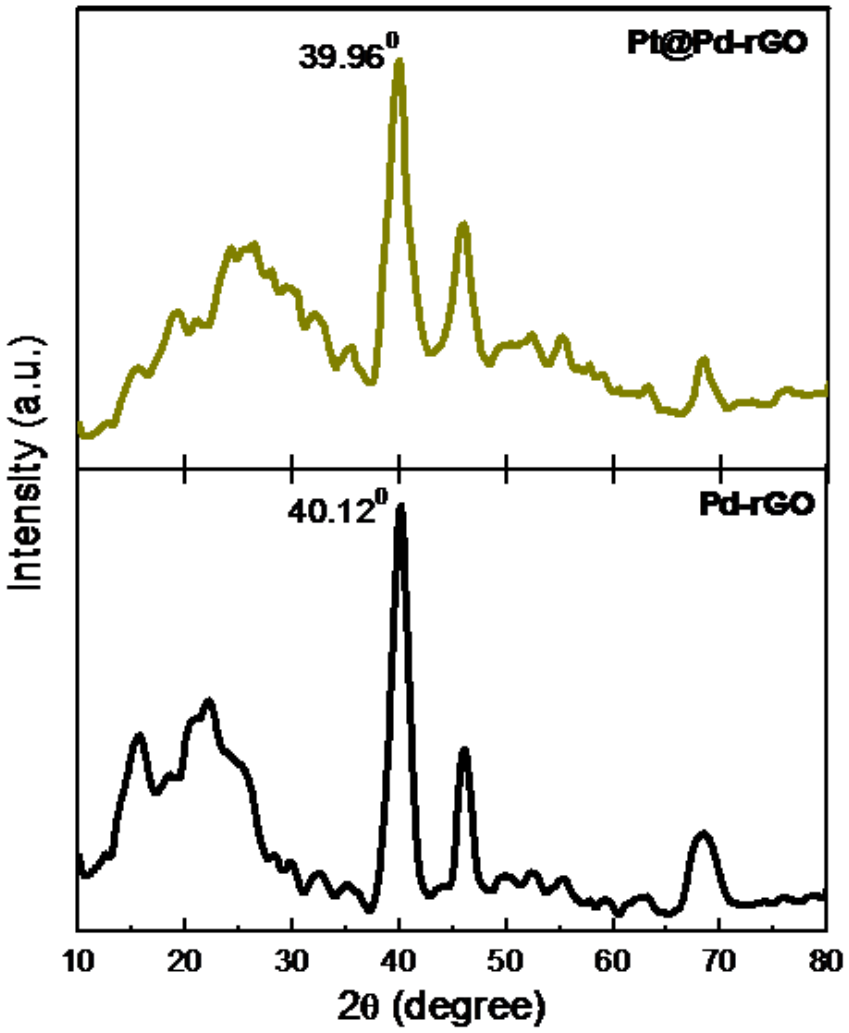

Figure 4. XRD spectrum of Pd/rGO and Pt@Pd/rGO catalysts.

Morphology and granulometric confirmation is also carried out by TEM and HRTEM analysis before and after Pt deposition over Pd-rGO NPs. HRTEM images showed the single phase crystallite formation after the deposition of Pt with lattice fringes values of 0.225 nm, corresponding to the Pt and Pd (111) facets (see Figure 3). More over the powder XRD spectra of Pd NPs provide the existence

ofPd (111) peak at 40.12^0 for Pd-rGO and 39.96^0 for Pt@Pd-rGO which is inbetween the Pd and Pt (111) peaks, also confirms the formation of single phase bimetallic nanocomposite (see Figure 4).

In the electrochemical deposition process, the solution containing H_2PtCl_6 as precursor salt, the cathodic limit for the experiments was selected to be −0.2V to 0.15 V (vs Ag/AgCl), which is slight negative to the hydrogen evolution potential where Pt particles reduced on the surface of Pd NPs leading to H_2 evolution during the electro-deposition phenomenon. The CV corresponding to Pt deposition shows that reduction of Pt NPs starts at about 0.05 V (vs Ag/AgCl) and the obtained corresponding current increases due to the reaction, as the potential limit shifts to more negative values, facilitating a mass transport controlled process [22]. The layer by layer cycles of deposition CVs demonstrated the smooth and uniform deposition of Pt on Pd NPs. Besides, the final CV segment is coupled with released hydrogen ions on Pt atoms. Pletcher and co-workers [23] believe that these CV segments can be completely explained by slow reduction of Pt atoms into zero valent Pt NPs, where the solution contains a saturated amount of $PtCl_6^{2-}$ and two species such as $(PtCl_5(H_2O)^-$and $PtCl_4(H_2O)_2)$ resulting from the hydrolysis reaction, the each species reduced to Pt(0) NPs [24].

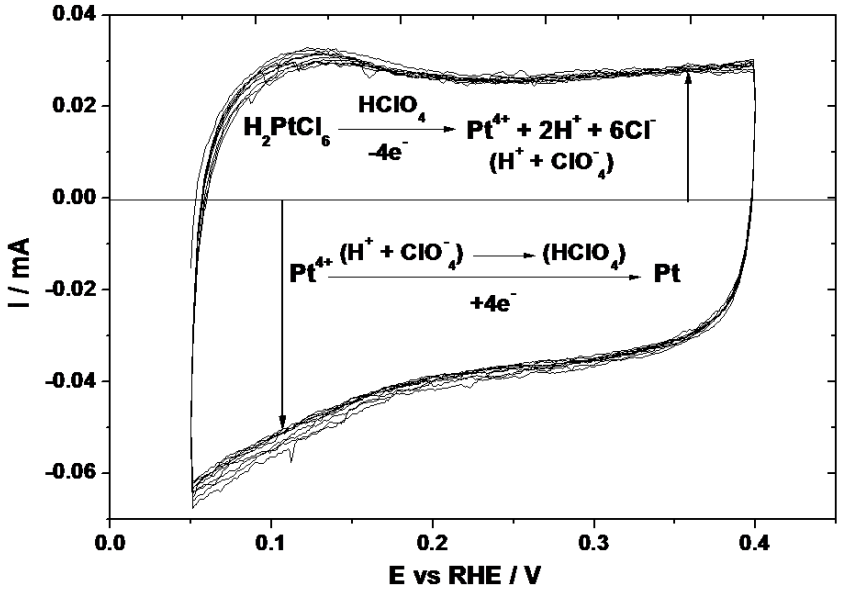

Figure 5. Electrochemical deposition of Pt on Pd-rGO NPs by potential cycling method in 0.1M $HClO_4$+0.1M H_2PtCl_6 solution at 50 mV/s, with mechanism at positive scans and negative scans.

The above explained interpretation highly coincides with the multiple segments observed in CV cycles (Figure 5), although the presence of Pt(+II) as a stable intermediate cannot be discarded. It is known that the over potential of Pt is much lower, so Pt can be deposited on GO supported Pd NPs at a lower over potential favored kinetically by Pt nuclei formed at carbon support [25]. Above whole phenomenon with mechanism is presented in Figure 5. After the deposition of Pt on Pd-rGO NPs their LSV and CV are presented in Figures 7-A and 7-B respectively, which are showing a strong characterization proof for Pt coverage over Pd-rGO NPs. The shapes of the curves in both the figures

demonstrate the essential changes with Pt deposition on base material. Two quasireversible peaks in H_{ads} region between intervals 0.05 to 0.30V are observed. The current in doble layer region increases, oxygen desorption peak is weakly pronounced. The specific surface area is increased after the deposition of Pt NPs. As the Pt NPs are deposited on Pd-rGO base material the size of catalyst is increased and ultimately the specific surface area which depends on mass loading of metals also increased. So the current in Pt@Pd-rGO CV is higher than that of Pd-rGO. The presence of Pt on Pd-rGO base material was later analysed by EDX analysis given in figure 6. EDX analysis is showing the presence of Pt with ultra-low loading along with Pd material.

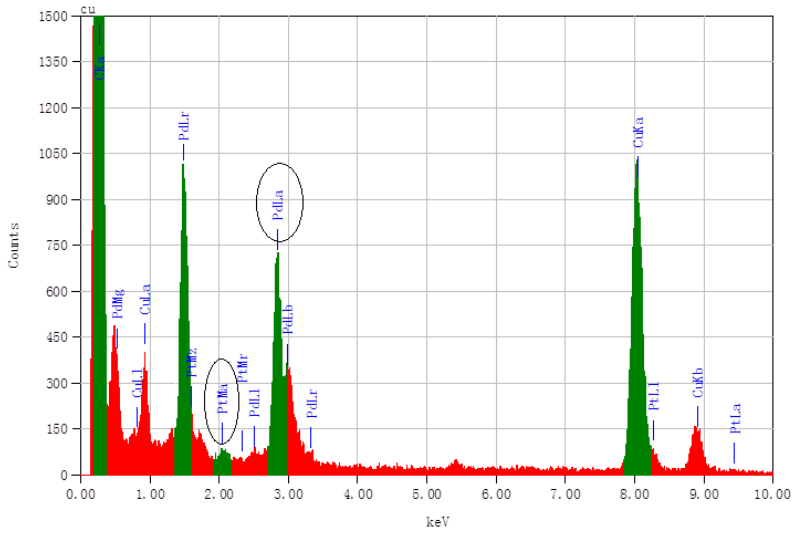

Figure 6. EDX analysis for Pt@Pd-rGO catalyst, which is showing presence of Pt and Pd. Atomic composition of Pd:Pt is 90.24:9.76 showing ultra-low loading of Pt.

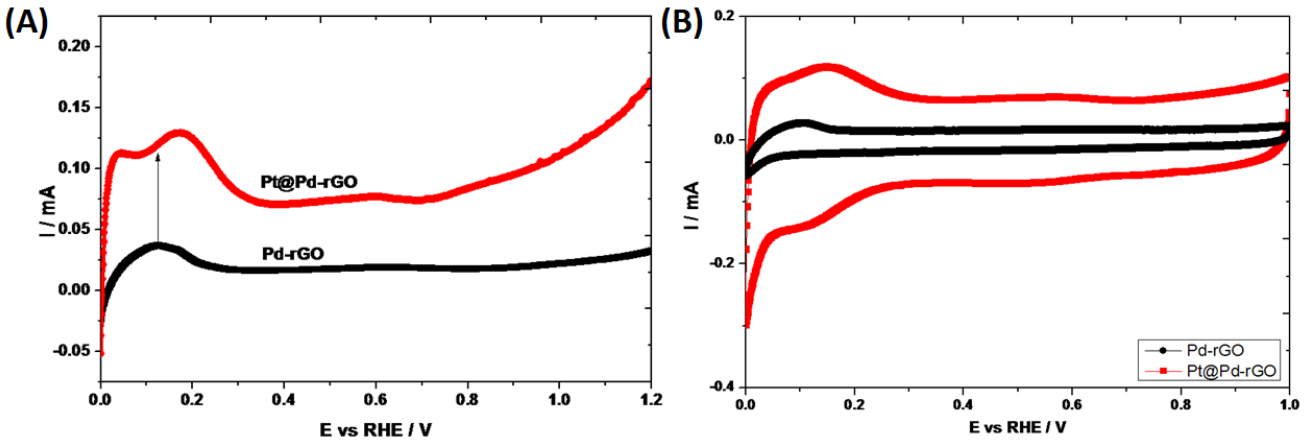

Figure 7. (A) LSV for Pd-rGO NPs and after deposition of Pt on them Pt@Pd-rGO NPs in 0.1M $HClO_4$ solution at 50 mV/s and **(B)** Base CVs for Pd-rGO NPs and after deposition of Pt on them Pt@Pd-rGO NPs in 0.1M $HClO_4$ solution at 50 mV/s.

The electrocatalytic activity towards methanol oxidation reaction (MOR) is measured for as synthesized Pd-rGO and electrochemically deposited Pt@Pd-rGO catalysts. It is clear that the specific activity, onset potential and current density is increased by deposition of very little amount of Pt. Among these two catalysts, Pd-rGO and Pt@Pd-rGO showed the highest current densities with a value of about 250 µA cm^{-2} and 3250 µA cm^{-2} respectively, which is much higher improvement after Pt deposition. Also the MOR activity is compared with 20% wt commercial Pt/C (see figure 8). The basic mechanism for the improvement of MOR activity is as follows. After the deposition of Pt on Pd-rGO, a bimetallic composite type catalyst is obtained. In this catalyst the Pt is responsible for the chemisorption of methanol and Pd for the oxidation of water species. Pt will adsorb the intermediate carbonaceous species like CO_{ads} and Pd will adsorb its counter intermediate specie like OH_{ads}. As in PdPt bimetallic composite the d-bands centers of Pt shifts down and Pt-CO_{ads} bonding become weaker, at the same time Pd-OHads reacts with it and eventually leads the formation of CO_2. Thus, the methanol oxidation process enhance in bimetallic composite catalyst in this work. Moreover, higher tolerance to the CO_{ads} poisoning of electrocatalysts generally evaluated by the forward (If) to backward current density (Ib) ratio values [26-28].

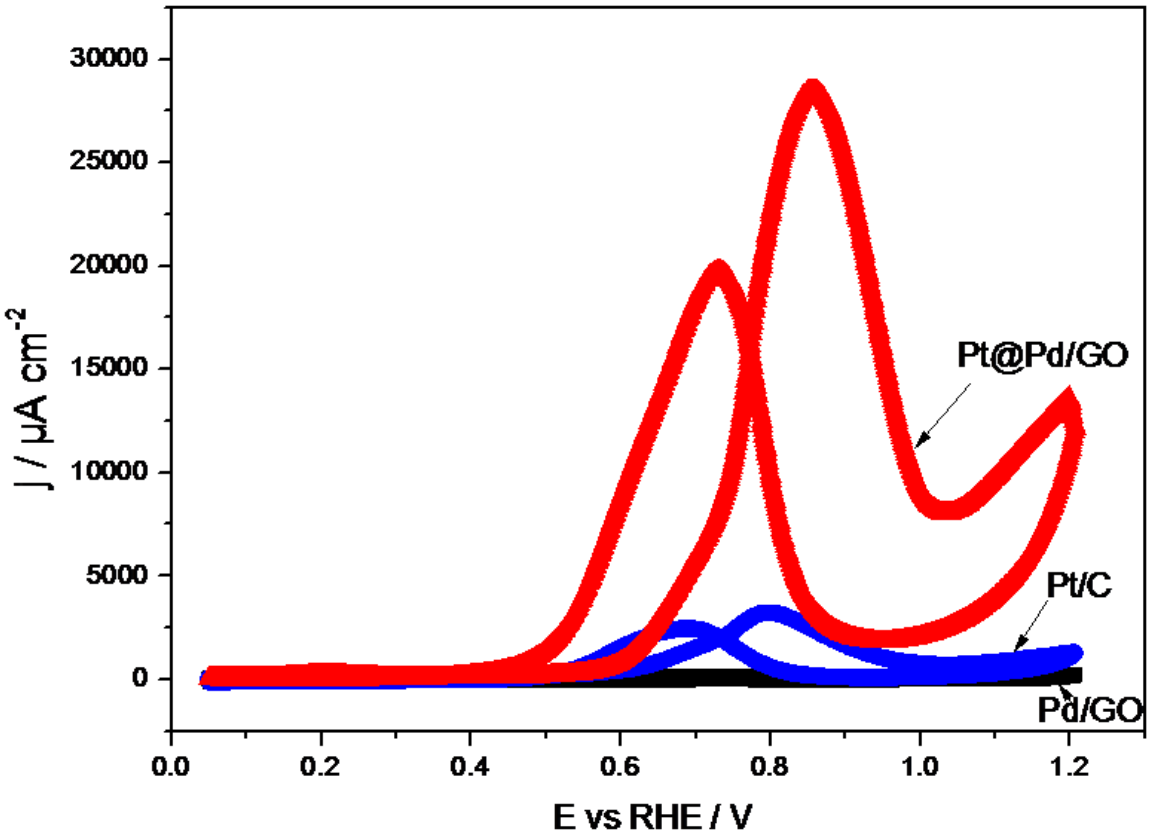

Figure 8. MOR activity for Pd-rGO, Pt@ Pd-rGOand 20% wt commercial Pt/C in 1M CH_3OH+0.1M $HClO_4$ solution at 50 mVs.

In Comparison to the prior catalyst, the later (Pt@Pd-rGO) showed higher If/Ib ratio values, indicating that the mutual contribution of Pd Pt and also the corporation of Pt into the Pd-rGO NPs, the catalyst could reduce the CO poisoning during the reaction, which is demonstrated in Figure 9. In this figure the high value of If/Ib ratio indicates that most of the CO_{ads} intermediate carbonaceous species were oxidized to CO_2 in forward scan due to the presence of OH_{ads} on Pd sites in surrounding, leading to a negligible poisoning of Pt sites. The onset potential for MOR activity is a much important parameter for a good catalyst. Lower the value of onset potential greater the activity of the catalyst is considered. In the present work the onset potential for MOR is significantly shifted towards the negative side. The prior catalyst has onset potential lower than 0.7V and the later catalyst has lower than 0.5V vs RHE.

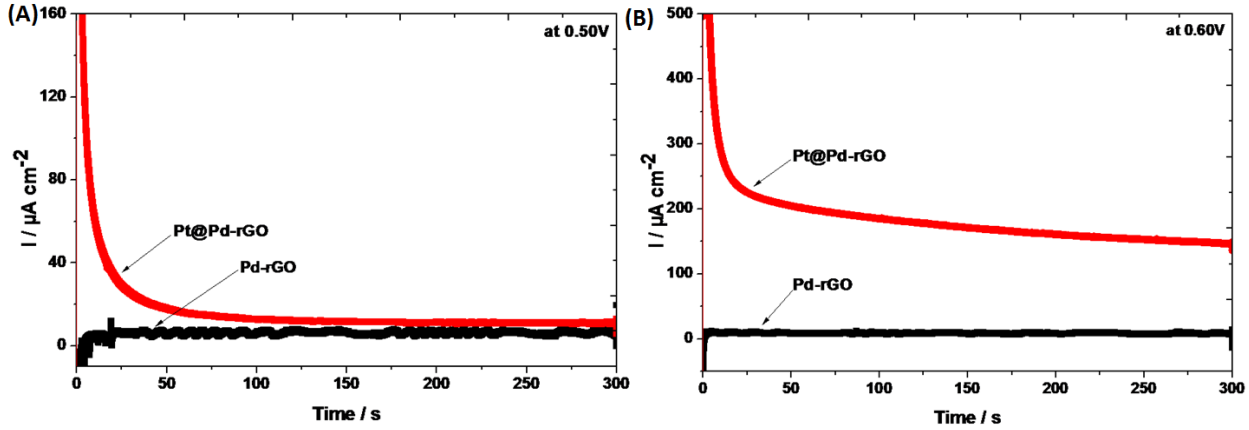

Figure 9. Chronoamperometric result of MOR activity for Pd-rGO and Pt@ Pd-rGO in 1M CH_3OH+0.1M $HClO_4$ solution **(A)** at constant potential of 0.50V and **(B)** at constant potential of 0.60V

This shift of onset potential for oxidation of methanol towards lower values is a good massage in this field of research. To make more strengthen these results, the chronoamperometric results for MOR activity are also presented at 0.5V and 0.6V vs RHE in Figures 9-A and 9-B respectively. The enhanced performance of the Pt@Pd-rGO catalyst for MOR attributed to the bi-functional process [28-30]. For the present nanocatalyst, Pt active sites were responsible for methanol chemisorptions to form $Pt–CH_3OH_{ads}$ leading to $Pt\text{-}CO_{ads}$, whereas Pd catalyzed the dehydrogenation of water molecules to form $Pd–OH_{ads}$, resulting in the oxidation of the strongly adsorbed CO_{ads} species on the active sites by the reaction between $Pt–CO_{ads}$ and $Pd–OH_{ads}$. The strong coupling between Pd-Pt atoms can also reduce the coordination between Pt and $–CO_{ads}$ bonds thereby, breaking Pt-COads. These synergistic effects highly enhanced the overall performance of Pt@Pd-rGO catalyst.

4. CONCLUSION

In conclusion, we have synthesized clean surfactant free rGO supported Pd NPs by using CO as reducing and capping agent. Then highly active catalyst for electrocatalytic activity of MOR and with

better tolerance to CO poisoning caused during MOR is developed by electrochemical deposition of Pt on Pd-rGO NPs. This facile route is of great significance for the synthesis of Pd-based catalysts directly on GC electrodes surfaces. Lastly, the present information revealed that nanocatalyst fabricated on three dimensional substrates such as rGO support could be of great interest for a number of applications in renewable and sustainable energy devices with electrochemical synthesis of nanocatalysts.

ACKNOWLEDGEMENTS
Ammar Bin Yousaf and Rashid Khan contributed equally to this work. This work is supported by USTC fellowship programme offered by University of Science and Technology of China, Hefei and Anhui Government Scholarship offered by Anhui provincial government China.

References

1. P. Strasser, S. Koh, T. Anniyev, J. Greeley, K. More, C. F. Yu, Z. C. Liu, S. Kaya, D. Nordlund, H. Ogasawara, M. F. Toney and A. Nilsson, *Nat Chem.*, 2 (2010) 450.
2. Z. Liu, Q. Shi, F. Peng, H. Wang, R. Zhang, H. Yu, *Electrochem commun.*,16 (2012) 73.
3. K. Zhang, Q. Yue, G. Chen, Y. Zhai, L. Wang, H. Wang, J. Zhao, J. Liu, J. Jia and H. Li, *J. Phys. Chem. C*, 115 (2011) 379.
4. J. Sun, Y. Wang, C. Zhang, T. Kou and Z. Zhang, *Electrochem. Commun.*, 21 (2012) 42.
5. Q. J. Wang and J. G. Che, *Physical Review Letters*,103 (2009) 066802.
6. X. Chen, G. Wu, J. Chen, X. Chen, Z. Xie and X. Wang, *J. Am. Chem. Soc.*, 133 (2011) 3693.
7. J.C. Claussen, A.D. Franklin, A. Haque, D. M. Porterfield and T.S. Fisher, *ACS Nano*, 3 (2009) 37.
8. M. Zhou, Y. Wang, Y. Zhai, J. Zhai, W. Ren, F. Wang and S. Dong, *Chemistry-A European Journal*, 15 (2009) 6116.
9. J. Szanyi, W. K. Kuhn and D. W. Goodman, *J. Vac. Sci. Technol.*, 11 (1993) 1969.
10. L. Li, M. Chen, G. Huang, N. Yang, L. Zhang, H. Wang, Y. Liu, W. Wang and J. Gao, *J. Power Sources*, 263 (2014) 13-21.
11. W. K. Kuhn, J. Szanyi and D. W. Goodman, *Surf. Sci.*, 274 (1992) 611.
12. A. B. Anderson and M. K. Awad, *J. Am. Chem. Soc.*, 107 (1985) 7854.
13. Q. Li, Z. Zhou, R. Chen, B. Sun, L. Qiao, Y. Yao and K. WuInsights, *Phys. Chem. Chem. Phys.*, 17 (2015) 9126-9134.
14. A. M. Bradshaw and F. M. Hoffmann, *Surf. Sci.*,72 (1978) 513.
15. W. K. Kuhn, J.Szanyi, and D. W. Goodman, *Surf. Sci. Lett.*, 274 (1992) 611.
16. E. Ozensoy, D. C. Meier and D. W. Goodman, *J. Phys. Chem. B*, 106 (2002) 9367−9371.
17. H. Ohtani, M. A. Van-Hove and G. A. Somorjai, *Surf. Sci*., 187 (1987) 372−386.
18. T. Giebel, *Surf. Sci.*, 406 (1998) 90−102.
19. S. Surnev, M. Sock, M. G. Ramsey, F. P. Netzer, M. Wiklund, M. Borg and J. N. Andersen, *Surf. Sci.*, 470 (2000) 171−185.
20. M. K. Rose, T. Mitsui, J. Dunphy, A. Borg, D. F. Ogletree, M. Salmeron and P. Sautet, *Surf. Sci.*, 512 (2002) 48−60.
21. N. M. Martin, M. V. den-Bossche, H. Gronbeck, C. Hakanoglu, F. Zhang, T. Li, J. Gustafson, J. F. Weaver and E. Lundgren, *J. Phys. Chem. C*, 118 (2014) 1118−1128.
22. M. M. E. Duarte, A. S. Pilla, J. M. Sieben and C. E. Mayer, *Electrochem. Commun.*, 8 (2006) 159 164.
23. H. M. Yasin, G. Denuault, D. Pletcher, *J. Electroanal. Chem.*, 633 (2009) 327–332.
24. J. M. Sieben, *Mater. Chem. Phys.*, 128 (2011) 243–249.

25. C. Bock, C. Paquet, M. Couillard, G. A. Botton, B. R. MacDougall, *J. Am. Chem. Soc.*, 126 (2004) 8028–8037.
26. Z. Liu, X. Ling, X. Su and J. Lee, *J. Phys. Chem. B*, 108 (2004) 8234.
27. H. Wang, S. Chen, C. Wang, K. Zhang, D. Liu, Y. A. Haleem, X. Zheng, B. Ge and Li Song *J. Phys. Chem. C*, 120 (2016) 6569–6576.
28. L. Minmin, R. Zhang and W. Chen, *Chem. Rev.*, 114 (2014) 5117–5160.
29. F. Zhan, T. Bian, W. Zhao, H. Zhang, M. Jin and D. Yang, *Cryst. Eng. Comm.*, 16 (2014) 2411 2416.
30. J. Rossmeisl, P. Ferrin, G. Tritsaris, A. Nilekar, S. Koh, S. Bae, S. Brankovic, P. Strasser and M. Mavrikakis, *Energy Environ. Sci.*, 5 (2012) 8335.

© 2016 The Authors. Published by ESG (www.electrochemsci.org). This article is an open access article distributed under the terms and conditions of the Creative Commons Attribution license (http://creativecommons.org/licenses/by/4.0/).